

Impact of Hadronic Backgrounds on Selected Higgs Physics Analyses at a Linear Collider

K. DESCH¹, A. IMHOF^{1,2}, N. MEYER^{1,2}, A. RASPEREZA²

¹ *Institut für Experimentalphysik, Universität Hamburg, Luruper Chaussee 149,
D-22761 Hamburg, Germany*

² *DESY, Notkestrasse 85,
D-22607 Hamburg, Germany*

Abstract

We perform an initial study of the impact of hadronic events from the collision of beamstrahlung photons on selected Higgs Boson analyses at a linear collider at center-of-mass energies of 500 GeV and 1 TeV. Particular emphasis is given to the fact that background events from many bunch crossings may pile up if the detector is not able to tag single bunch crossings at a very short bunch crossing time. Studied processes are SM Higgs production in the 4-jet channel and the reconstruction of Higgs decays into tau-lepton pairs at $\sqrt{s} = 500$ GeV and the selection of Higgs bosons decaying into a $b\bar{b}$ pair in the WW-fusion process at $\sqrt{s} = 1$ TeV. Both the situation at a superconducting machine (TESLA) and a normal-conducting machine (NLC) are compared. At the NLC we find a severe degradation of the achievable precision if the time-stamp capability of the detector is significantly worse than 5.6 ns, corresponding to four bunch crossings.

1 Introduction

At a future linear e^+e^- collider with high luminosity, unlike as at previous e^+e^- machines, the interaction of colliding bunches cannot be viewed as collisions of single electron-positron pairs. Due to the high charge density, the bunch collisions rather have to be investigated as a whole. The dominant effect of these collisions is beamstrahlung, i.e. radiation of photons off the colliding electrons/positrons in the electro-magnetic field of the positron/electron bunch. The beamstrahlung photons are produced at very low angles and leave the detector through the beam-pipe. The dominant effects from beamstrahlung which affect the experiment are the following:

1. Energy loss of the incoming particles leading to a broad energy distribution of the incoming beams. The size of the effect is similar to that of initial state radiation (ISR) of the colliding particles.
2. Creation of e^+e^- -pairs from beamstrahlung photons: these pairs typically have low transverse momentum. With a high magnetic field (more than 3 T) the largest fraction can be kept inside the beam-pipe. However, a fraction of these pairs hits the most forward part of the detector, the luminosity calorimeter (BeamCAL). Furthermore, the produced particles may hit detector or machine parts where additional particles may be produced and backscatter into the sensitive detector volume. Additionally, a small fraction of these pairs has sufficient transverse momentum to produce tracks and clusters in the detector directly.
3. Creation of hadrons, $\gamma\gamma \rightarrow \text{hadrons}$ from colliding beamstrahlung photons. Although much lower in rate than the e^+e^- pair creation background this process has a tail to higher transverse momenta which can produce physical hits also in the central detector. Furthermore, also neutral particles (mainly π^0 's) are produced which cannot be collimated into the forward region by the magnetic field.

The effect of beamstrahlung background in terms of additional occupancy of detector components [1] and the resulting difficulties in pattern recognition and event reconstruction has been studied in detail [2]. In this note we study only the impact of the $\gamma\gamma \rightarrow \text{hadrons}$ process on physics analyses. An earlier study for the TESLA case has been presented in [3].

One particular aspect of the present analysis is the possibility of accumulating background from more than one bunchcrossing if the detector is not able to tag the reconstructed particle flow objects (i.e. reconstructed charged and neutral particles) with their associated bunch crossing number. Bunch tagging of particle flow objects can be done by using timing information of the associated hits in all contributing detector components (vertex detector, central tracker, calorimeter). Since a large part of the additional background particles is neutral, the time tagging capability of the calorimeter alone is of particular importance.

The bunch schemes for a superconducting LC (TESLA) and for a normal-conducting LC (NLC/GLC) are very different. At TESLA, the bunch separation is 337/176 ns at 500/800 GeV. At the NLC/GLC, the time between two subsequent bunches is 1.4 ns. Therefore, the effort needed to do an efficient bunch tagging is more challenging at a warm machine. In order to find out which level of bunch tagging is needed to ensure minimal impact on the detector performance for precision measurements, we perform this study as a function of the number of bunch crossings which cannot be tagged individually, ranging from 1 to 64. Bunch tagging at the 100 ns level is achieved in current detectors, e.g. at HERA and at the Tevatron. The LHC experiments strive for a tagging resolution of 25ns, i.e. the LHC bunch spacing to prevent large pile-up. For the NLC/GLC detector the aim is to achieve a time stamping resolution corresponding to a few NLC/GLC bunch crossings.

As long as the occupancy of single detector cells is low for a single bunch no pile-up will occur in individual cells. Then it is sufficient to tag (time-stamp) the corresponding hits. If the occupancy approaches one, i.e. if the probability that the same detector cell (or in case of collective time-tagging of showers) neighboring cells within a typical shower

radius) is hit in consecutive bunch crossings, time-stamping is not sufficient. Rather has the detector to be read out completely after a bunch crossing. This situation may occur in the very forward region but it is not studied in this note.

In Section 2, we describe the time structure of the beams at TESLA and at NLC/GLC and the four scenarios which are considered in this note. In Section 3 we outline the simulation procedure and describe the general properties of overlaid $\gamma\gamma \rightarrow$ hadrons events. We consider three different Higgs physics channels with different requirements for the detector performance: the measurement of the Higgs mass in the $HZ \rightarrow b\bar{b}q\bar{q}$ channel (Section 4) and the reconstruction of the $H \rightarrow \tau^+\tau^-$ decay (Section 5) at $\sqrt{s} = 500$ GeV, and the study of the WW-fusion process, $e^+e^- \rightarrow H\nu\bar{\nu}$ at $\sqrt{s} = 1$ TeV (Section 6).

2 Time Structure and Beam Parameters

The time structure of the LC beams is characterized by the following parameters:

- the number of bunches per train,
- the time between two bunches,
- the train repetition rate.

These parameters are specific to the linac options (warm/cold). The beam parameters assumed in this study are given in Tab. 1 for the TESLA and NLC/GLC machines. They are taken from the International Technical Review Committee (ILC-TRC) report [4].

	TESLA		NLC/GLC	
	500 GeV	800 GeV	500 GeV	1 TeV
Number of bunches per train	2820	4886	192	
Bunch separation (ns)	337	176	1.4	
Bunch train length (μ s)	950	860	0.267	
Average number of $\gamma\gamma \rightarrow$ hadrons / BX*	0.248	0.399	0.103	0.270

Table 1: Beam parameters for TESLA and NLC/GLC as outlined in the ILC-TRC Report [4]. For TESLA, we use the 800 GeV parameters also for 1 TeV. *The number of background events corresponds to events with $\gamma\gamma$ center-of-mass energy in excess of 5 GeV.

The hadronic background is specified in terms of the average number of background events overlapping with one recorded physical event. When the detector is not able to tag single bunches, this quantity, denoted hereafter $\langle N_{\gamma\gamma \rightarrow had} \rangle$, can be expressed as

$$\langle N_{\gamma\gamma \rightarrow had} \rangle = n_{\gamma\gamma \rightarrow had}^{bx} \frac{\sigma_t}{\Delta t_b},$$

where $n_{\gamma\gamma \rightarrow had}^{bx}$ is the average number of $\gamma\gamma \rightarrow$ hadrons events per bunch crossing, σ_t is the detector tagging resolution and Δt_b is the time separation between bunches. If the detector is able to resolve two adjacent bunches, the average number of background events overlapping with one physical events is solely defined by the average number of these events per bunch crossing, $\langle N_{\gamma\gamma \rightarrow had} \rangle = n_{\gamma\gamma \rightarrow had}^{bx}$.

Four scenarios are studied in this note. The first scenario is based on the conditions expected at TESLA. Given the relatively large bunch separation we assume that adjacent bunches can be disentangled. The average number of background events for this scenario is 0.25 (0.4) at center-of-mass energy of 500 (1000) GeV.

The other three scenarios assume NLC/GLC beam parameters. In the following three scenarios we assume that bunch tagging can be performed for 4/18/64 bunch crossings. The scenarios differ in the assumptions made on the tagging time resolution. The first scenario suggests that the detector time resolution corresponds to 4 bunch crossings, resulting in 0.4 (1.1) overlaid background events at $\sqrt{s} = 500$ (1000) GeV. The second scenario takes as a reference the typical time resolution of the LHC detectors, $\sigma_t \sim 25$ ns, leading to $\langle N_{\gamma\gamma \rightarrow had} \rangle = 1.8$ (4.8) at $\sqrt{s} = 500$ (1000) GeV. The third scenario assumes integration over a third of a bunch train, leading to 6.4 (17.3) overlaid background events at $\sqrt{s} = 500$ (1000) GeV. The four scenarios are summarized in Tab. 2.

Scenario	Machine	# BX	Tagging resolution	$\langle N_{\gamma\gamma \rightarrow had} \rangle$	
				500 GeV	1000 GeV
1	TESLA	1	337/176 ns	0.25	0.4
2	NLC/GLC	4	5.6 ns	0.4	1.1
3	NLC/GLC	18	25 ns	1.8	4.8
4	NLC/GLC	64	89 ns	6.4	17.3

Table 2: The number of integrated bunch crossings, the corresponding detector tagging resolution and the average number of overlaid background events for the four scenarios investigated in the present note. Note that the total bunch charge differs for the different machines.

3 Simulation

The simulation of hadronic $\gamma\gamma$ -interactions from the beamstrahlung photons is performed in three steps:

1. Energy and position of the colliding photons are simulated with GUINEA-PIG [5]. Bunch sizes and accelerator parameters are taken into account during this step. We assume perfect beams.
2. The process $\gamma\gamma \rightarrow$ hadrons is simulated with PYTHIA [6]. A cut of 5 GeV is applied to the two-photon center-of-mass energy W . The PYTHIA default process set MSEL=2 is used. This contains hard QCD scattering, semi-hard QCD-processes as well as diffractive scattering. It has been shown recently [7] that events with $W < 5$ GeV yield further charged and neutral particles entering the detector. They are neglected in this study.
3. The HADES library [8] is used to overlay a poisson distributed number of two-photon events to hard physics processes simulated separately. The mean numbers of overlaid events are listed in Tab. 2. They are based on numbers in the ILC-TRC report which were produced for the same cut in W .

Detector effects are simulated by the fast Monte Carlo SIMDET [9]. The event properties of the background events were cross checked with the GEANT-based full simulation BRAHMS [10]. Fig. 1 shows the distributions of the visible energy and the charged multiplicity for the case of 6.4 average overlaid background events at $\sqrt{s} = 500$ GeV. Good agreement between fast and full simulation is observed at this level. For the physics studies presented in this note we use SIMDET.

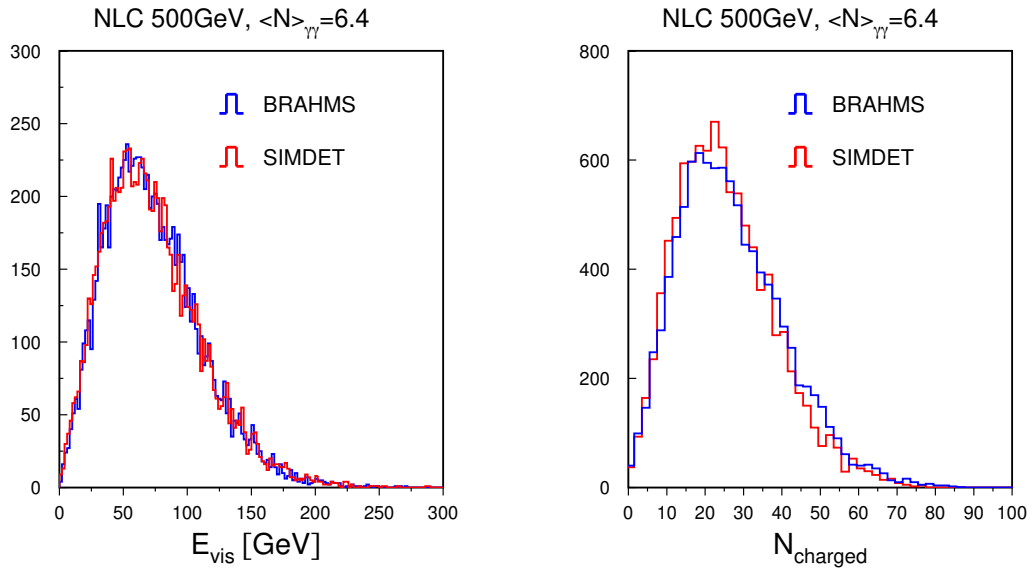


Figure 1: Total visible energy (left) and number of reconstructed charged particles (right) of hadronic two-photon background corresponding to scenario 4 (64 BX at NLC/GLC) at 500 GeV. The blue (dark) line shows the GEANT3 based full detector simulation BRAHMS, the red line is for the fast parametric Monte-Carlo SIMDET.

Particles produced in soft hadronic $\gamma\gamma$ interactions are mostly low-energetic. Only every twentieth of such events contains particles with $E > 5$ GeV. The energy spectrum is shown in Fig. 2 (top left). In addition, particles from overlaid events are produced under small polar angles predominantly. The difference arising from the different beam parameters of NLC and TESLA are small. Fig. 2 (top right) shows the expected additional energy deposition. The distributions for an accumulated average number of background events according to scenarios 1-4 are shown in the lower part of Fig. 2.

In order to minimize the impact of overlaid background, selection criteria at the level of particle flow objects are most promising. Cuts, however, cannot be defined globally but depend on the hard physics process under study. In each of the studied physics analyses, the measures to suppress effects from background have been adjusted differently, taking into account the expected signal properties as well.

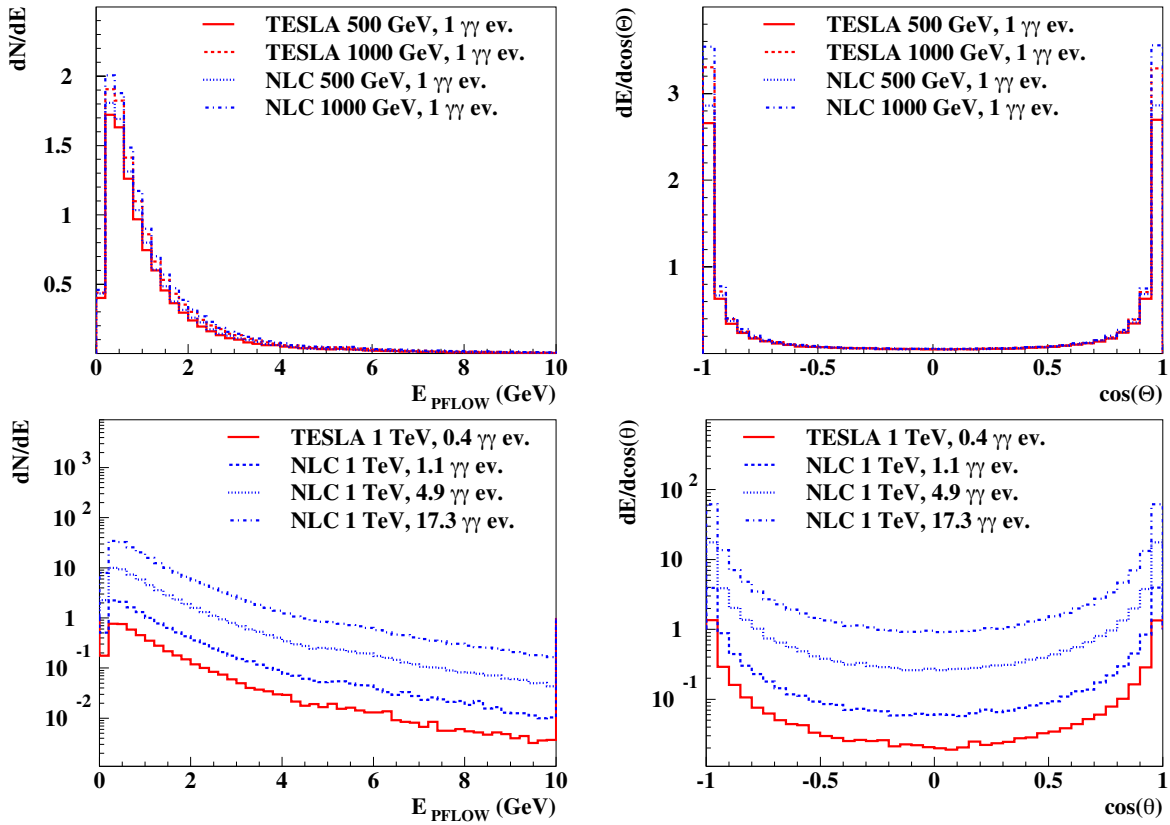


Figure 2: Expected particle energy spectrum (left) and energy weighted $\cos \theta$ distribution (right) from hadronic two-photon background. The upper plots are for one background event at TESLA and NLC for 500 and 1000 GeV respectively. The bottom plots show the accumulated distributions corresponding to scenarios 1-4.

4 Reconstruction of the Higgs Boson Mass in the 4-jet Channel at 500 GeV

We have chosen the $e^+e^- \rightarrow HZ \rightarrow b\bar{b}q\bar{q}$ channel to evaluate the impact of $\gamma\gamma \rightarrow \text{hadrons}$ background on the Higgs boson mass measurement. Previous studies performed for center-of-mass energy of 350 GeV demonstrated that the $HZ \rightarrow b\bar{b}q\bar{q}$ channel provides the best statistical accuracy of the mass measurement, $\delta m_H = 45$ MeV, for the SM Higgs boson with mass $m_H = 120$ GeV [11]. These studies, however, did not take into account the $\gamma\gamma \rightarrow \text{hadrons}$ background. In this note a similar study for $m_H = 120$ GeV is performed at $\sqrt{s} = 500$ GeV including the $\gamma\gamma \rightarrow \text{hadrons}$ background for scenarios 1-4. We also study the impact of the $\gamma\gamma \rightarrow \text{hadrons}$ background on the separation of the Higgs signal from the dominant $ZZ \rightarrow q\bar{q}q\bar{q}$ background.

The assumed integrated luminosity is 500 fb^{-1} . The Higgs-strahlung cross-section for $m_H = 120$ GeV at $\sqrt{s} = 500$ GeV is 65.9 fb including initial state radiation according to HPROD [12] leading to about 15200 events expected in the $HZ \rightarrow b\bar{b}q\bar{q}$ channel. The cross-section of the $ZZ \rightarrow q\bar{q}q\bar{q}$ background process, calculated with PYTHIA, is 340 fb yielding about 170000 events.

Initially, the study is performed without applying any special criteria to reduce the $\gamma\gamma \rightarrow \text{hadrons}$ background. A simplified selection was applied to accept high multiplicity hadronic events compatible with a 4-jet topology. Each event should pass the following selection criteria.

- The number of particle flow objects has to be larger than 20.
- The total energy deposited in the detector must be larger than 400 GeV.
- A soft cut on the event thrust, $T < 0.95$, rejects two- and three-jet events while preserving high signal efficiency.
- A cut on the polar angle of the thrust vector, $|\cos \theta_T| < 0.95$, separates $WW \rightarrow q\bar{q}q\bar{q}$ and $ZZ \rightarrow q\bar{q}q\bar{q}$ events, which are peaking in the forward/backward region, from the centrally produced HZ events.
- The event is forced into four jets using the Durham cluster algorithm [13] and the b-tag variable, a measure of the likelihood to contain a B-hadron, is computed as described in Ref. [14] for each jet. The two highest b-tag variables are required to be larger than 0.5.

In the next step a kinematic fit is applied to improve the mass resolution of the reconstructed particles using the package developed by the DELPHI Collaboration [15]. We require four-momentum conservation and constrain one of the two dijet masses to the mass of the Z boson, $m_Z = 91.2$ GeV. This leads to a five constraint fit (5C-fit). There are six possibilities to assign the four jets to a Higgs boson and a Z boson. Out of the six possible jet pairings, the one which minimizes the χ^2 of the kinematic fit is chosen. The effect of the kinematic fit is illustrated in Fig. 3. In Fig. 4 the reconstructed Higgs mass

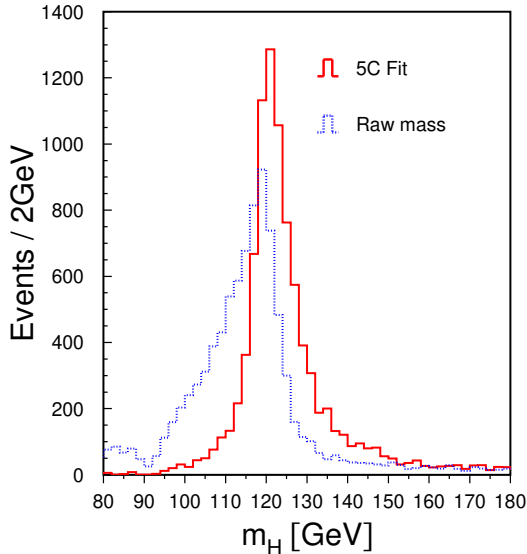


Figure 3: The reconstructed Higgs mass distribution obtained using measured jet energies and angles (dotted line) and with 5C kinematic fit described in text (solid line). No $\gamma\gamma \rightarrow \text{hadrons}$ background is overlaid.

distribution obtained for no overlaid background is compared with the four background scenarios.

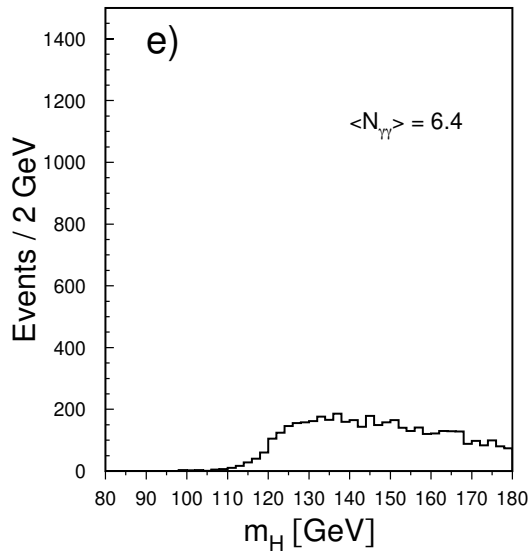
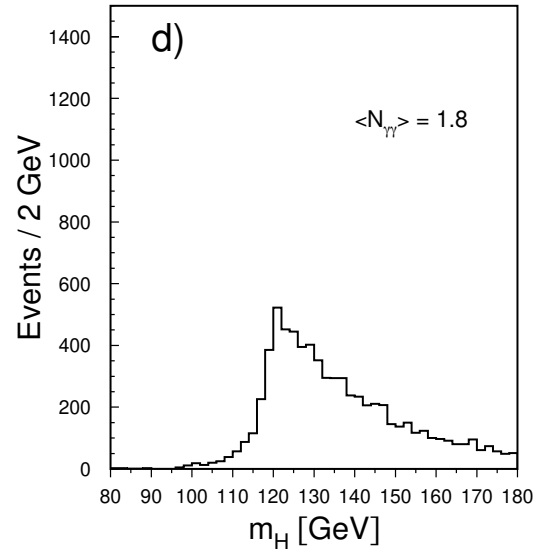
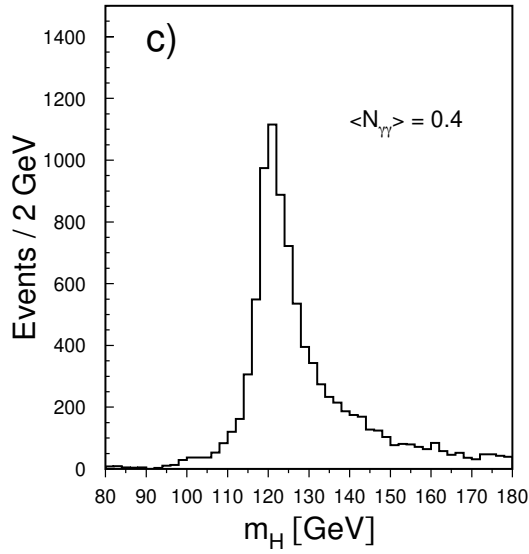
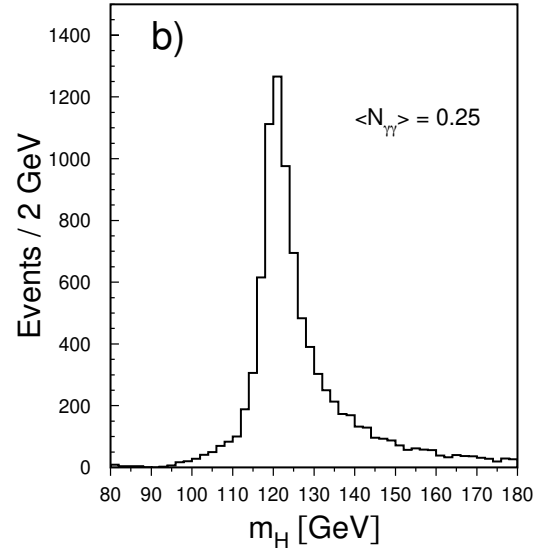
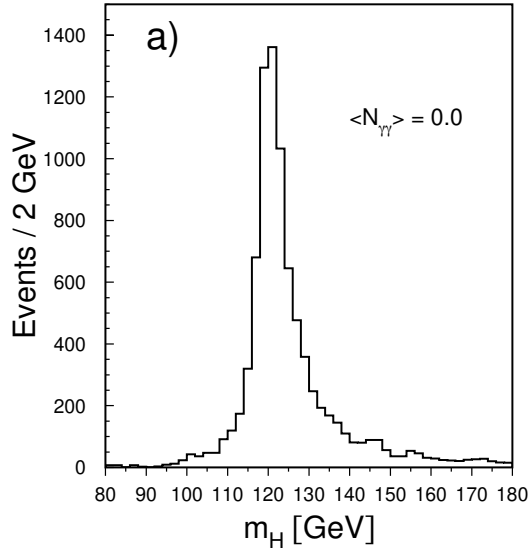


Figure 4: The Higgs mass distribution in the case of no overlaid background events (a) and for 0.25, 0.4, 1.8 and 6.4 overlaid background events, scenarios 1-4 (b-e). No special cuts are applied to reduce the effect of $\gamma\gamma \rightarrow \text{hadrons}$ background.

A significant degradation of the mass resolution is observed already for 1.8 overlapping background events (scenario 3), and for 6.4 overlapping events (scenario 4) no distinct peak in the mass spectrum can be seen. To improve the analysis in the presence of background, additional cuts are introduced which reduce $\gamma\gamma$ background contamination for each e^+e^- event. A large fraction of the excess energy from the piled-up background events is carried by low p_t particles. Therefore we reject particle flow objects with transverse momentum p_t less than 1 GeV. This cut is not applied in the case of 0.25 overlaid events (scenario 1) and relaxed to 0.5 GeV for 0.4 overlaid events (scenario 2). An additional cut makes use of correlation between energy and polar angle of the particles originating from hadronic $\gamma\gamma$ interactions. As mentioned in Section 3, particles from $\gamma\gamma \rightarrow \text{hadrons}$ events are predominantly produced at low polar angles. Furthermore, particles produced at low angles are typically more energetic. Therefore each particle flow object is required to fulfill

$$|\cos \theta_{pflow}| < 1.0 - A \exp(-E_{pflow}/E_0), \quad (1)$$

where θ_{pflow} is the polar angle of the particle flow object and E_{pflow} is its reconstructed energy. The parameters A and E_0 are optimized separately for each scenario to maximize the statistical significance of the signal expressed as

$$S = N_S / \sqrt{N_S + N_B},$$

where N_S and N_B are the numbers of the $HZ \rightarrow b\bar{b}q\bar{q}$ and $ZZ \rightarrow q\bar{q}q\bar{q}$ events with the reconstructed Higgs mass in the window $110 \text{ GeV} < m_H^{\text{rec}} < 130 \text{ GeV}$. Particle flow objects not satisfying criterium (1) are rejected. The cuts to reduce the $\gamma\gamma \rightarrow \text{hadrons}$ background contamination are summarized in Tab. 3.

scenario	$\langle N_{\gamma\gamma \rightarrow \text{had}} \rangle$	P_T	A	E_0 [GeV]
1	0.25	–	0.05	2
2	0.4	$> 0.5 \text{ GeV}$	0.07	3
3	1.8	$> 1 \text{ GeV}$	0.10	5
4	6.4	$> 1 \text{ GeV}$	0.15	10

Table 3: Cuts reducing background from overlaid $\gamma\gamma \rightarrow \text{hadrons}$ events.

After applying these cuts, each event is subjected to the selection criteria described before. The presence of background as well as specific cuts rejecting background contamination are found to have a strong impact on jet energy and angular resolution functions employed in the kinematic fit. Therefore resolution functions are derived separately for each of the considered scenarios by comparing reconstructed jet energies and angles with the energies and angles of generated quarks. It was found that this procedure result in improvement of Higgs mass resolution. Obtained resolution functions are listed in Table 4.

The effect of the background rejection on the analysis performance is shown in Figure 5 for scenario 3 ($\langle N_{\gamma\gamma \rightarrow \text{had}} \rangle = 1.8$). It can be seen, that the signal mass resolution can be partially recovered, but not to the level obtainable in absence of the background.

Figure 6 presents the reconstructed Higgs boson mass spectra for the case of no overlapping background events and for the four scenarios corresponding to 0.25, 0.4, 1.8 and

scenario	$\langle N_{\gamma\gamma \rightarrow had} \rangle$	σ_E/E	$\sigma_\theta, \text{ mrad}$	σ_ϕ
	0.0	$0.60/\sqrt{E/\text{GeV}}$	10	$\sigma_\theta/\sin\theta$
1	0.25	$0.70/\sqrt{E/\text{GeV}}$	10	
2	0.4	$0.75/\sqrt{E/\text{GeV}}$	10	
3	1.8	$0.90/\sqrt{E/\text{GeV}}$	11	
4	6.4	$1.20/\sqrt{E/\text{GeV}}$	12	

Table 4: Jet energy and angular resolution functions as derived separately for each scenario.

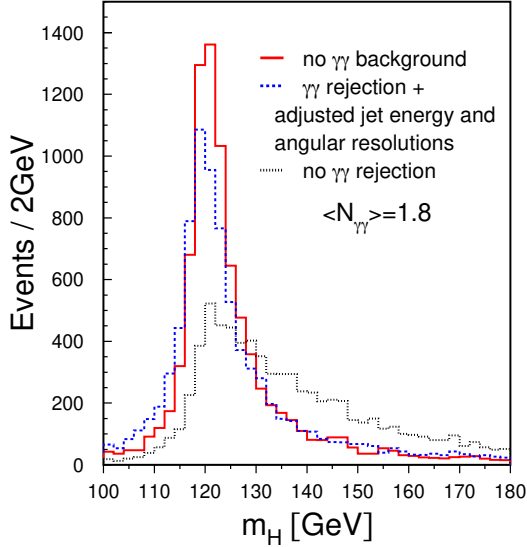


Figure 5: Distribution of the reconstructed Higgs boson mass in the $HZ \rightarrow b\bar{b}q\bar{q}$ sample in the case of no overlaid events (solid line) and in the case of 1.8 overlaid events (scenario 3) without applying background rejection (dotted line), with applying rejection and employing adjusted jet energy and angular resolution functions in the kinematic fit (dashed line).

6.4 overlapping background events. The $HZ \rightarrow b\bar{b}q\bar{q}$ signal is shown on top of the $ZZ \rightarrow q\bar{q}q\bar{q}$ background. Spectra are obtained after applying $\gamma\gamma$ background rejection.

The statistical accuracy of the Higgs boson mass measurement is obtained by fitting the mass spectra with a superposition of signal and background functions. The results are summarized in Tab. 5 in terms of the number of signal events (N_S), the number of $ZZ \rightarrow q\bar{q}q\bar{q}$ background events (N_B) in the mass window 110 – 130 GeV, the corresponding signal efficiency (ϵ) and statistical error on the Higgs boson mass (δm_H) for each of the scenarios considered. The statistical error on the Higgs boson mass degrades from 59 to 96 MeV with increasing average number of overlapping $\gamma\gamma$ events from 0 to 6.4. The deterioration of the precision of the Higgs mass measurement can be translated into a luminosity factor defined as

$$F_{\mathcal{L}} = \mathcal{L}^*/\mathcal{L}_0,$$

where \mathcal{L}^* is the luminosity needed to reach the same statistical accuracy as in the case of no overlapping events with the nominal luminosity, $\mathcal{L}_0 = 500 \text{ fb}^{-1}$. This factor increases from 1.1 to 2.3 with $\langle N_{\gamma\gamma \rightarrow had} \rangle$ increasing from 0.25 to 6.4.

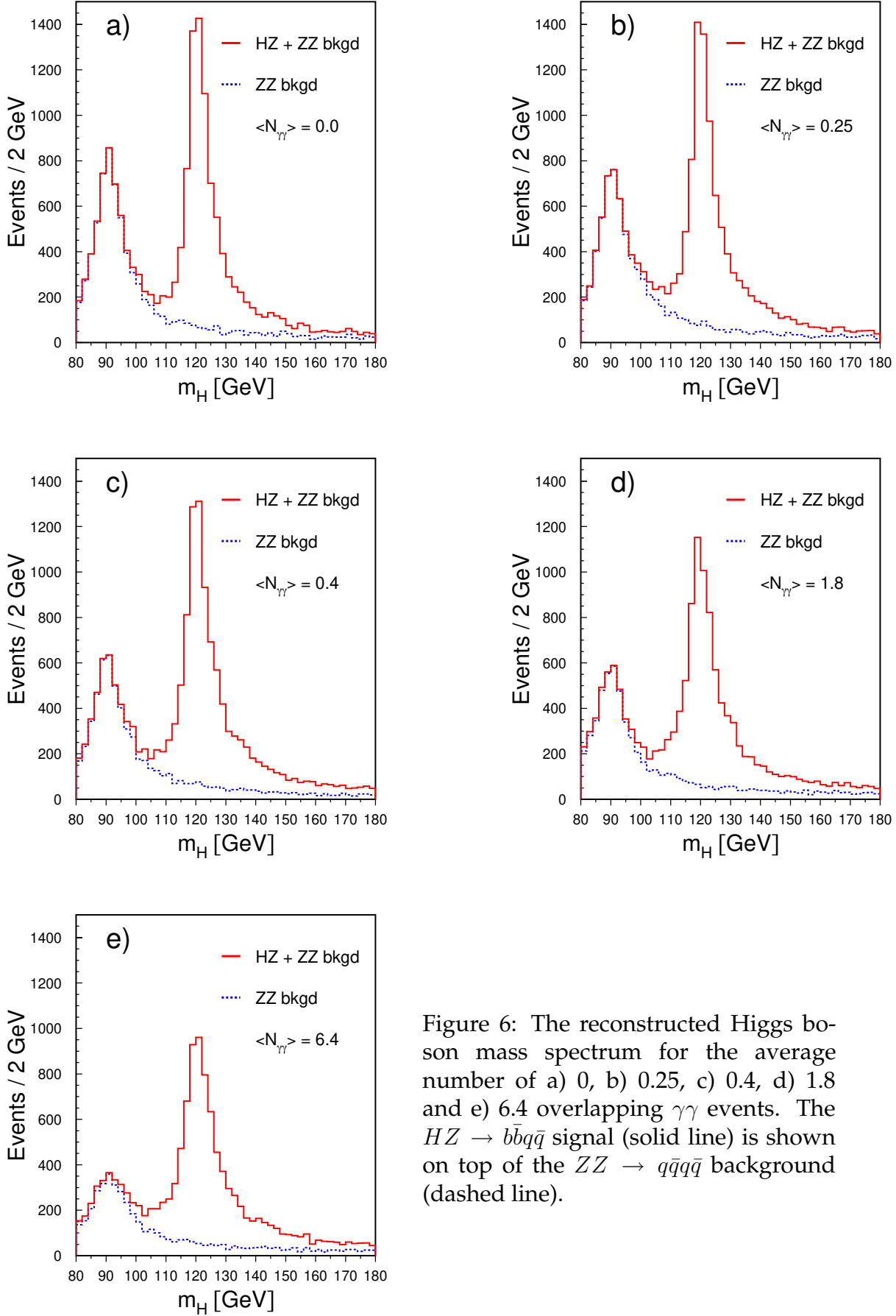


Figure 6: The reconstructed Higgs boson mass spectrum for the average number of a) 0, b) 0.25, c) 0.4, d) 1.8 and e) 6.4 overlapping $\gamma\gamma$ events. The $HZ \rightarrow b\bar{b}q\bar{q}$ signal (solid line) is shown on top of the $ZZ \rightarrow q\bar{q}q\bar{q}$ background (dashed line).

	$\sqrt{s} = 500 \text{ GeV}, \quad m_H = 120 \text{ GeV}, \quad \mathcal{L}_0 = 500 \text{ fb}^{-1}$					
scenario	$< N_{\gamma\gamma \rightarrow \text{had}} >$	N_S	ϵ	N_B	$\delta m_H [\text{MeV}]$	$\mathcal{L}^*/\mathcal{L}_0$
	0.0	6460	42.5%	720	59	–
1	0.25	6310	41.5%	830	62	1.1
2	0.4	6400	42.1%	690	70	1.4
3	1.8	5730	37.7%	675	80	1.7
4	6.4	5285	34.7%	580	96	2.3

Table 5: The number of signal events (N_S), $ZZ \rightarrow q\bar{q}q\bar{q}$ background events (N_B) in the mass window 110 – 130 GeV, the corresponding signal efficiency (ϵ), the statistical error on the Higgs boson mass (δm_H) and the luminosity factor $\mathcal{L}^*/\mathcal{L}_0$ defined in the text. The numbers are given as a function of $< N_{\gamma\gamma \rightarrow \text{had}} >$.

5 Reconstruction of $H \rightarrow \tau^+\tau^-$ Decays

The Higgs boson parity can be measured by investigating transverse spin correlations in the decay $H \rightarrow \tau^+\tau^-$ [16]. The experimental analysis of these spin correlations involves the exclusive reconstruction of hadronic τ decays. We have studied in particular the reconstruction of $\tau^- \rightarrow \rho^- \bar{\nu}_\tau \rightarrow \pi^- \pi^0 \bar{\nu}_\tau \rightarrow \pi^- \gamma \gamma \bar{\nu}_\tau$. From the reconstructed four-momenta of the final-state pions of both τ decays the acoplanarity angle between the two ρ decay planes has to be calculated [17].

To study the impact of overlaid hadronic $\gamma\gamma$ events we consider Higgs bosons produced in the Higgs-strahlung process at $\sqrt{s} = 500 \text{ GeV}$ for $m_H = 120 \text{ GeV}$ and 1 ab^{-1} of integrated luminosity. The analysis will be statistics limited and therefore requires a very efficient reconstruction of exclusive τ decays. Overlaid $\gamma\gamma \rightarrow \text{hadrons}$ background may in particular spoil the π^0 reconstruction.

The identification of the τ^\pm decay-products is based on a cone-selection, where a single isolated track which is not identified as electron or muon and with more than 2 GeV reconstructed energy is required inside an isolation cone. Inside a second smaller cone, the τ cone, around the π^\pm -candidate the energy of neutral objects is accumulated and associated with the π^0 decay into 2 photons. The neutral energy inside the inner cone is required to be above 1 GeV.

In order to minimize the impact of overlaid $\gamma\gamma \rightarrow \text{hadrons}$ background, we varied the sizes of both the outer and the inner cone for each of the four scenarios (see Tab. 6). The photons from the π^0 decays in the signal have a very broad energy spectrum. Around 13% of them have transversal momentum below 1 GeV. In this study only small fractions of the detector solid angle are used. Therefore a global $\gamma\gamma \rightarrow \text{hadrons}$ rejections by means of a cut on p_t is not applicable.

The effect of overlaid $\gamma\gamma \rightarrow \text{hadrons}$ background is three-fold. First, correctly identified τ leptons from Higgs decays may receive an additional background contribution leading to a shifted reconstructed ρ mass and diluted decay angle distribution. Second, good ρ candidates may be lost due to the isolation criterium. Third, additional ρ^\pm -candidates could be faked making the association of the ρ 's to Higgs boson ambiguous.

The distribution for the reconstructed invariant mass of the ρ candidates from signal events is shown in Fig. 7 for scenarios 1-4 and for the four different cone sizes. It can be seen that for cone size 1 ($15^\circ/10^\circ$) the number of reconstructed ρ 's decreases with increas-

	isolation cone	τ cone
cone size 1	15°	10°
cone size 2	10°	8°
cone size 3	8°	6°
cone size 4	6°	4°

Table 6: Different cone sizes applied in the τ identification (see text).

ing background. With decreasing cone size, the efficiency to reconstruct ρ 's in the absence of overlaid background decreases only slowly. However, with overlaid background, additional mainly low-mass ρ candidates appear. This can be also seen in Fig. 8, where the number of reconstructed ρ candidates is shown for the four cone sizes.

Since most of the additional candidates appear at low masses, we apply a cut at $m_\rho > 0.4$ GeV. To prevent candidates with too large mass from being accepted, also $m_\rho < 4$ GeV is required.

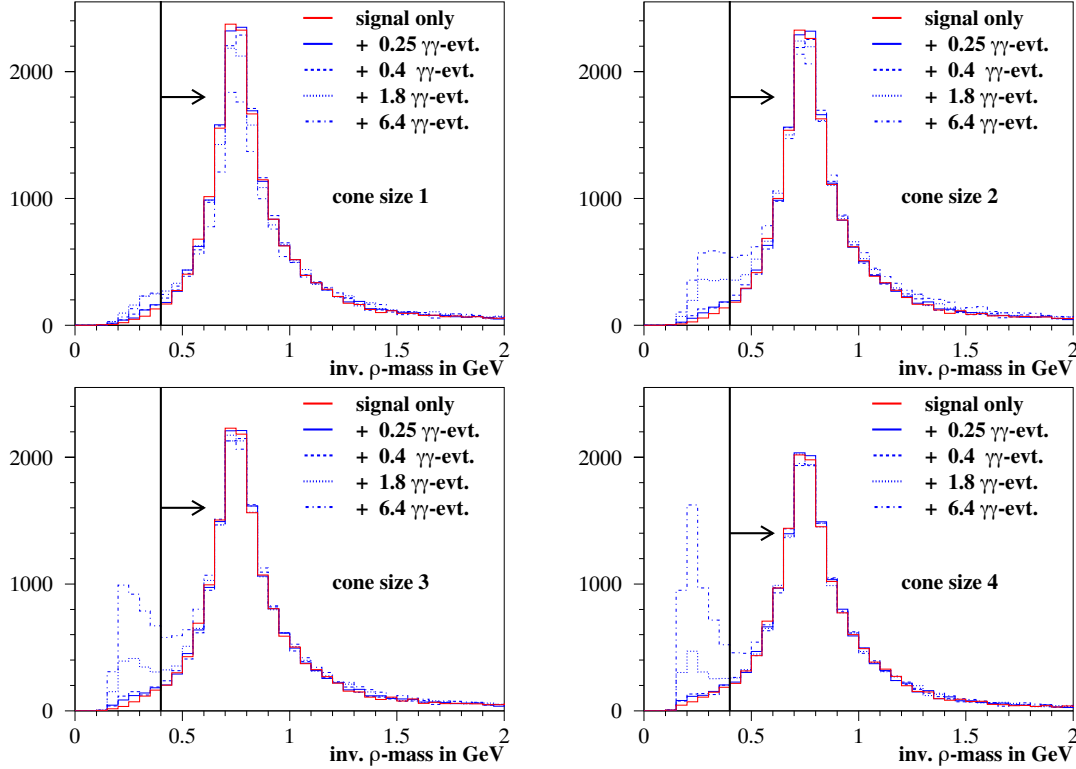


Figure 7: Reconstructed m_ρ^\pm distribution for no $\gamma\gamma \rightarrow \text{hadrons}$ background and scenarios 1-4. The four sub-figures correspond to four different cone-size applied in the τ identification. Candidates are accepted if $m_{\rho,\min} > 0.4$ GeV (black line).

If two or more cones are accepted, all opposite charge pairs are considered. Their invariant $\rho^+\rho^-$ -mass is shown in Figure 9. Events are accepted, if at least one combination satisfies $30 \text{ GeV} < m_{\rho\rho} < 115 \text{ GeV}$. It can be seen that the overlaid background causes a broadening of the $\rho^+\rho^-$ -mass distribution. Also ambiguities due to more than one ac-

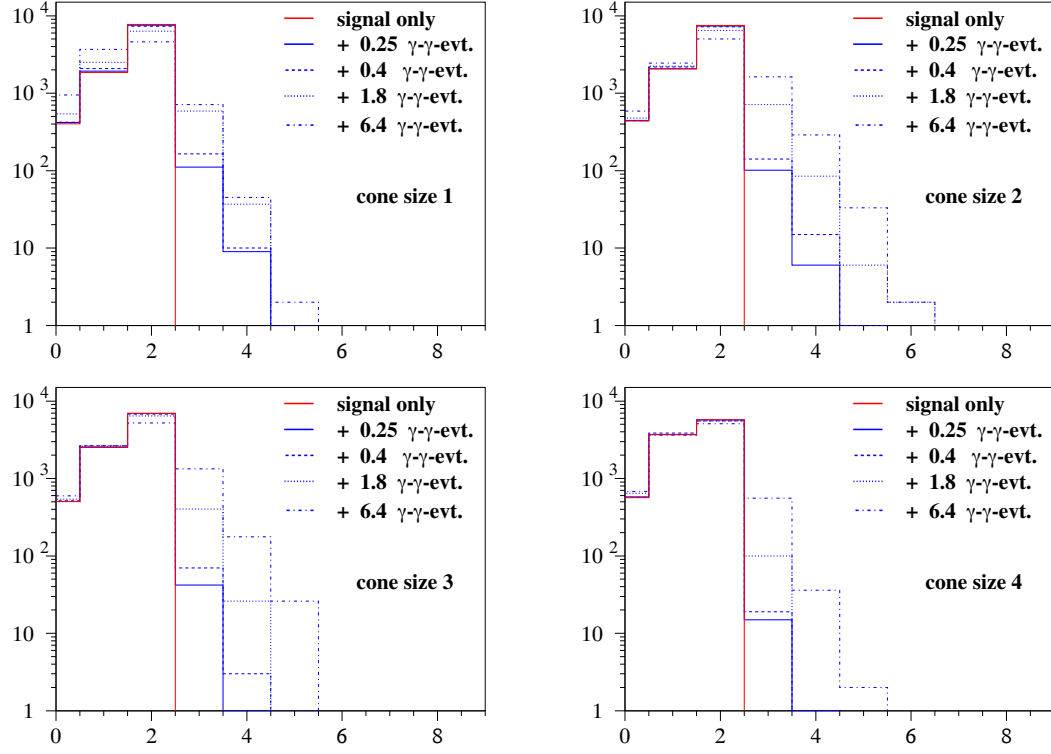


Figure 8: Number of reconstructed cones for the different scenarios before the cut on the cone-mass. The four sub-figures correspond to four different cone-sizes applied in the τ identification.

cepted pairing appear. In Tab. 7 the fraction of events which contain more than one good $\rho^+\rho^-$ pair is shown.

	Events with more than one accepted $\rho^+\rho^-$ pair			
	cone size 1	cone size 2	cone size 3	cone size 4
no BG	0%	0%	0%	0%
scenario 1	0.6%	0.4%	0.1%	0.1%
scenario 2	0.9%	0.7%	0.3%	0.1%
scenario 3	2.9%	3.3%	1.7%	0.3%
scenario 4	3.7%	8.3%	6.7%	2.3%

Table 7: Fraction of events which contain more than one good reconstructed $\rho^+\rho^-$ pair.

Only if *exactly* 2 ρ candidates are left which fulfill all selection criteria, the event is accepted for the calculation of the acoplanarity angle. This procedure might be optimized by a more sophisticated selection algorithm, e.g. based on the angles of the ρ candidates. In order to illustrate the impact of the overlaid background, the efficiency to find exactly one good $\rho^+\rho^-$ pair is shown in Tab. 8 and in Fig. 10 for the four considered cone-sizes and for the four background scenarios. It can be seen that using a smaller cone size in the presence of overlaid background the signal can partially be recovered. However, too small cone size will cut into the signal cones themselves. Since the analysis relies on high luminosity and is statistics-limited, a reduction in efficiency will always cause a loss in the measurement precision. The efficiency drops from above 70% for scenarios 1 and 2 down to around 50% for optimized cone sizes.

	cone size 1	cone size 2	cone size 3	cone size 4
no BG	75.0%	72.7%	67.5%	55.9%
scenario 1	73.3%	71.8%	67.2%	55.8%
scenario 2	71.4%	70.6%	66.1%	54.2%
scenario 3	62.7%	65.4%	63.8%	54.6%
scenario 4	44.4%	52.1%	53.8%	50.7%

Table 8: Selection efficiencies for different cone-sizes and overlaid events. Shown is the fraction of events, where exactly two reconstructed ρ^\pm candidates match all requirements mentioned in the text.

6 Higgs-Boson Production in WW-Fusion at 1 TeV

At high center-of-mass energy the number of beamstrahlung induced $\gamma\gamma \rightarrow$ hadrons event increases to 0.4 for TESLA at 800 GeV and to 0.27 at NLC/GLC at 1 TeV. We study the impact of the overlaid events on Higgs production through the WW-fusion process, $e^+e^- \rightarrow H\nu_e\bar{\nu}_e$. This process is the dominant source of Higgs bosons at high center-of-mass energies. A precise measurement of its cross-section is important to deduce the total Higgs boson width [18], yield an improved measurement of the Higgs branching

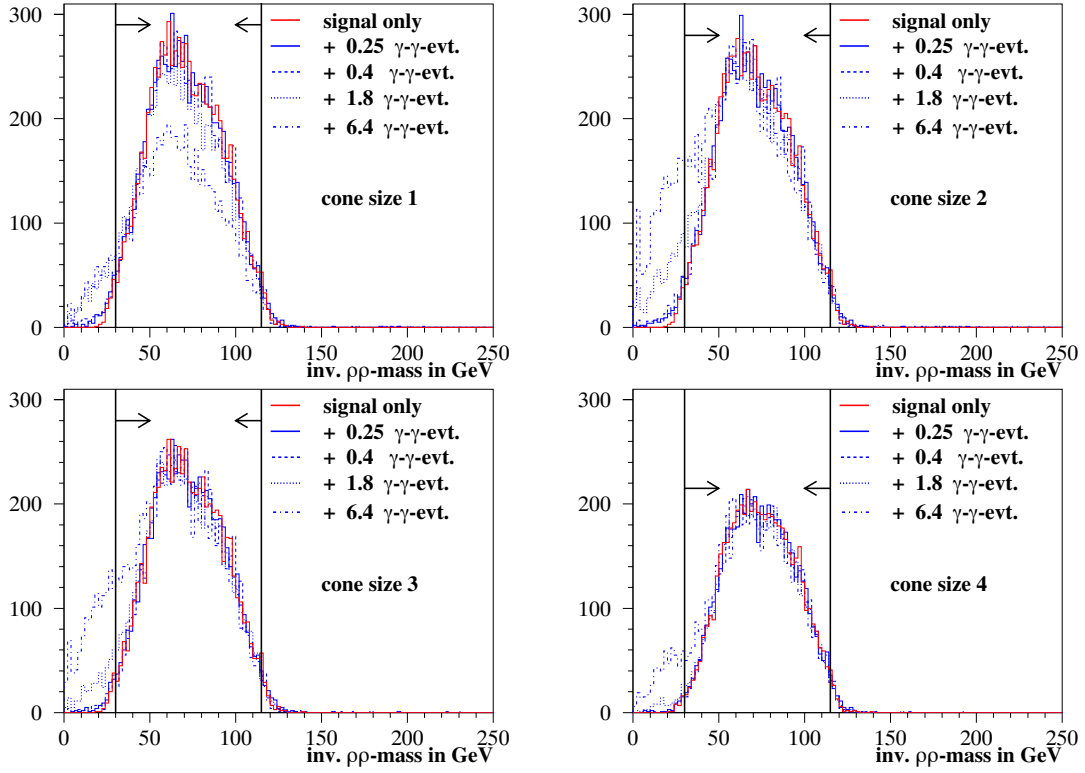


Figure 9: Reconstructed $\rho^+\rho^-$ mass for all ρ -pairs which have passed the cut on m_ρ^\pm and have opposite charge for the case of no $\gamma\gamma \rightarrow$ hadrons background and for scenarios 1-4. The four sub-figures correspond to four different cone-sizes applied in the τ identification.

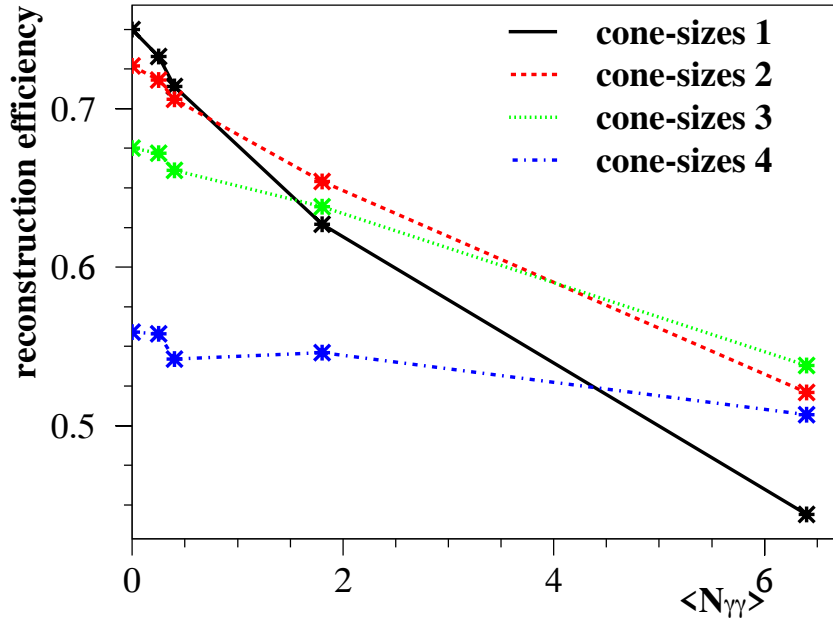


Figure 10: Reconstruction efficiency in dependence of the average number of overlaid $\gamma\gamma$ -events for the 4 different parameter-sizes studied.

ratios [19] and an improved global fit of Higgs couplings [20]. The study is performed for $m_H = 120$ GeV at $\sqrt{s} = 1$ TeV for the dominant $H \rightarrow b\bar{b}$ decay. The dominant background process is $e^+e^- \rightarrow Z\nu\bar{\nu} \rightarrow b\bar{b}\nu\bar{\nu}$. In order to reduce this background a precise measurement of the total visible mass is necessary. Kinematic constraints cannot be applied due to the missing neutrinos.

With additional particles from overlaid $\gamma\gamma \rightarrow$ hadrons events, the visible mass is strongly affected unless additional cuts are applied. Since particles from two-photon events are expected to have low transverse momentum, only reconstructed particles (particle flow objects) with $p_T > p_T^{min}$ are used to calculate the visible mass. However, a cut of p_T also affects parts of the jets from signal events leading to a decreasing mass resolution. The optimal value of p_T^{min} depends on the expected number of overlaid background events and is chosen such that less than 5 % of the accepted energy arises from background particles. Further possibilities to reduce the effect of overlaid background have not been applied in this study. One possibility might be to decompose the event into jets first and then only consider the regions around the jet axes. However, such a cone approach is problematic, since the fraction of accepted signal energy depends on jet fragmentation issues which introduce systematic uncertainties from QCD.

The $H\nu\bar{\nu}$ signal and the $Z\nu\bar{\nu}$ background are simulated with WHiZard [21] and then passed through the fast simulation SIMDET. In Fig. 11 (left) the remaining fraction of visible energy from background events (scenarios 1-4) and from the Higgs signal is shown as a function of p_T^{min} . In Fig. 11 (right) the background contamination, i.e. $E_B/(E_S + E_B)$ is shown. In order to achieve a background contamination of less than 5%, p_T^{min} has to be chosen between 0 and 1.6 GeV, as listed in Tab. 9.

scenario	1	2	3	4
$\langle N_{\gamma\gamma} \rangle$	0.4	1.1	4.9	17.3
p_T^{min} [GeV]	0.0	0.6	1.0	1.6

Table 9: Values for a cut on the transverse momentum, p_T^{min} of reconstructed particle flow objects.

The distributions of the visible mass after p_T^{min} -cuts are shown in Fig. 12 for the case of no $\gamma\gamma \rightarrow$ hadrons background and for scenarios 1-4. It can be seen that both the Higgs signal and the $Z\nu\bar{\nu}$ background peaks widen significantly with increasing number of overlaid background events.

In order to quantify the effect, signal and background events are counted within in a mass window of 30 GeV width around the signal peak. Since the signal mass peak does not only widen but also moves to lower values, the mass window position is adjusted such that the ratio of signal to $Z\nu\bar{\nu}$ -background events is maximized for each scenario. In Fig. 13 the number of signal events S (right) and the S/B ratio (left) are shown as a function of the number of bunch crossings the detector integrates. The numbers are normalized to scenario 1, i.e. to one bunch crossing with TESLA beam parameters. While the loss in signal events inside the mass window is marginal for scenario 2 (4 BX), a significant effect is observed for scenarios 3 and 4, for which S decreases by 15% or 17%, respectively. S/B decreases by 18% already for scenario 2 and by 31% (38%) for scenario 3 (4).

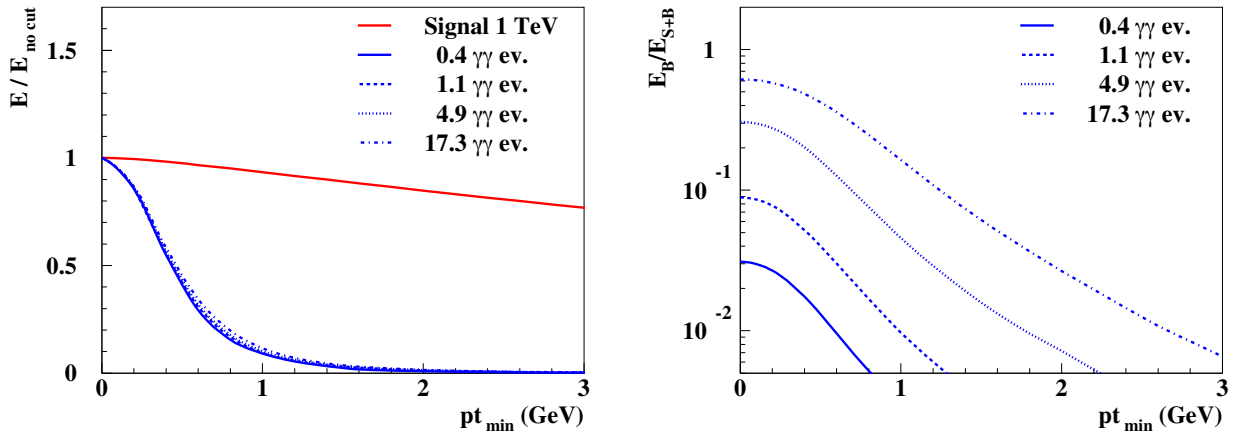


Figure 11: Dependence of the reconstructed energy on a cut on p_t : Left the ratio with respect to no cut for signal and various background scenarios separately, right the background contamination when signal and background are overlaid.

7 Summary and Conclusions

We have performed an initial study of the impact of beamstrahlung induced background from the process $\gamma\gamma \rightarrow \text{hadrons}$. We studied the case for TESLA beam parameters (scenario 1) where single bunches can be tagged by the detector. For NLC we consider the detector goal of integrating over 4 BX (5.6 ns) (scenario 2) and detectors with timing properties aimed for at LHC (scenario 3) and achieved at HERA (scenario 4). Our preliminary studies indicate that relaxing the NLC detector goal to scenario 3 (18 BX, 25 ns) would lead to a significant degradation of the achievable performance. We observed such a degradation in the precision on the Higgs mass and in the purity and efficiency of $H \rightarrow \tau^+\tau^-$ events needed to extract the Higgs CP quantum numbers at 500 GeV, and in the signal to background ratio achievable in the selection of $H\nu\bar{\nu}$ events at 1 TeV. Simple algorithms to reduce the impact of overlaid background have been applied. While the background can be significantly reduced by these algorithms, it was not possible to completely eliminate its impact on the physics performance. More sophisticated algorithms remain to be studied but they bear the risk of introducing new systematic uncertainties and biases into the analyses.

While certainly preliminary, we conclude that for a detector at NLC/GLC very fast time stamping ($\lesssim 10$ ns) is mandatory to maintain the desired physics performance. For a detector at TESLA this requirement is much more relaxed and can be achieved with today's technology.

References

- [1] C. Hensel, LC-DET-2000-001;
G. Wagner, LC-DET-2001-048;
K. Büser, O. Napoly, LC-M-2003-045.
- [2] T. Behnke *et al.*, LC-DET-2001-029.

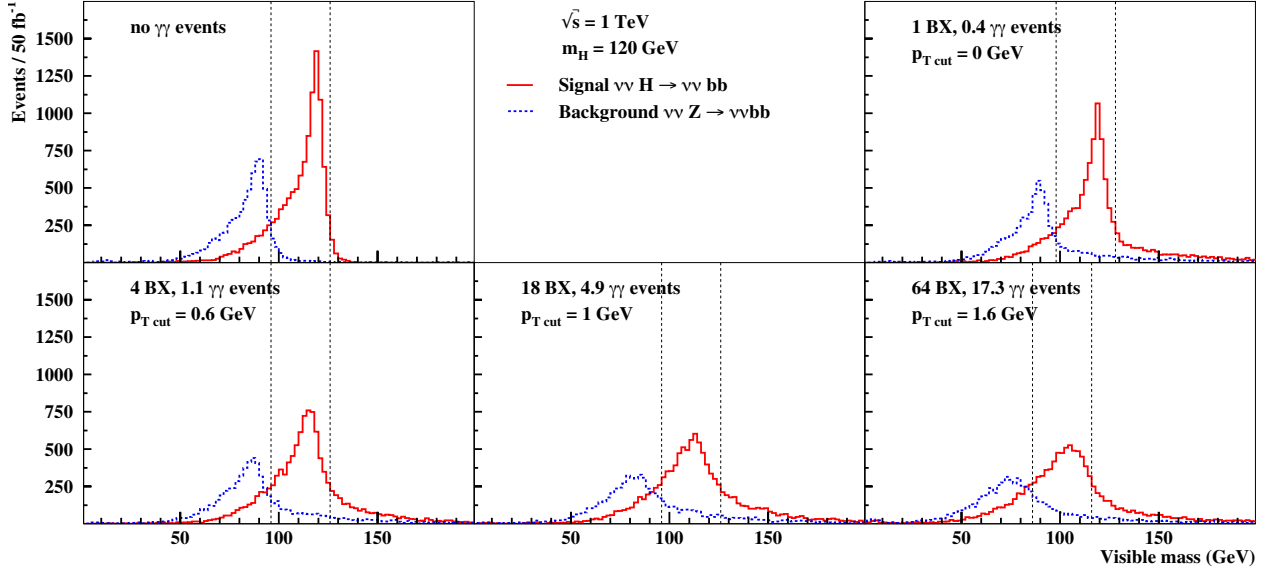


Figure 12: Visible mass of $H\nu\bar{\nu}$ signal events (red full line) and $Z\nu\bar{\nu}$ background events (blue dotted line) for the case of no overlaid background (upper left), scenario 1 (upper right) and scenarios 2-4 (lower row, left to right). An adjusted cut on p_T is applied for each scenario (see text).

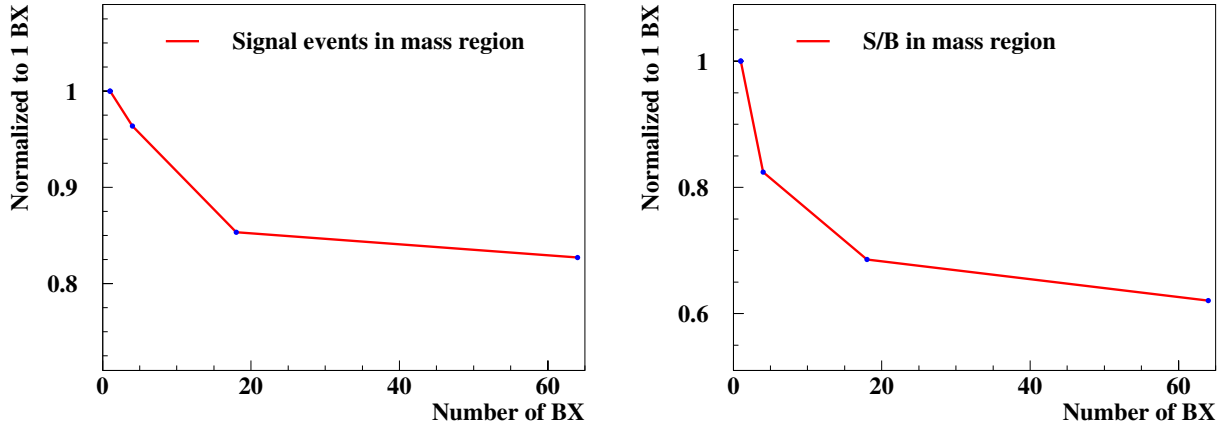


Figure 13: Number of signal events (left) and signal over background ratio (right) for scenarios 1-4 relative to the values for scenario 1. A mass window of 30 GeV around the signal peak position is applied.

- [3] M. Battaglia, D. Schulte, LC-PHSM-2000-052.
- [4] G. Loew et al., International Linear Collider Technical Review Committiee, ILC-TRC Report 2003,
<http://www.slac.stanford.edu/xorg/ilc-trc/2002/2002/report/03rephome.htm>
- [5] D. Schulte, PhD Thesis, TESLA 97-08 (1997).
- [6] T. Sjostrand, L. Lonnblad, S. Mrenna, hep-ph/0108264.
- [7] T. Barklow, "Update on Gamma-gamma to hadrons calculation", talk given at the ALCPG meeting, SLAC, Jan. 2004.
- [8] D. Schulte, HADES library,
<http://dschulte.home.cern.ch/dschulte/physics/hades/hades.html>
- [9] M. Pohl and H.J. Schreiber, DESY-02-061, LC-DET-2002-005 (2002).
- [10] T. Behnke et al., LC-TOOL-2001-005.
- [11] P. Garcia-Abia, W. Lohmann, A. Raspereza, LC-PHSM-2000-062.
- [12] A. Djouadi, "HPROD: A program for SM and MSSM Higgs boson production in e^+e^- collisions",
<http://w3.lpm.univ-montp2.fr/~djouadi/GDR/programs/hprod.html>.
- [13] S. Catani, Yu.L. Dokshitzer, M. Olsson, G. Turnock and B.R. Webber, Phys. Lett. B269 (1991) 432.
- [14] K. Desch, T. Klimkovich, T. Kuhl, A. Raspereza, "Study of Higgs Boson Pair Production at Linear Collider", LC-PHSM-2004-006.
- [15] N. Kjaer and R. Moller, "Reconstruction of Invariant Masses In multi-jet Events", DELPHI Note 91-17 PHYS 88.
- [16] M. Kramer, J. H. Kuhn, M. L. Stong and P. M. Zerwas, Z. Phys. C **64** (1994) 21;
B. Grzadkowski and J. F. Gunion, Phys. Lett. B **350** (1995) 218.
- [17] G. R. Bower, T. Pierzchala, Z. Was and M. Worek, Phys. Lett. B **543** (2002) 227, hep-ph/0204292.
- [18] K. Desch, N. Meyer, LC-PHSM-2001-025.
- [19] T. L. Barklow, arXiv:hep-ph/0312268.
- [20] K. Desch, M. Battaglia, LC-PHSM-2001-053.
- [21] W. Kilian, LC-TOOL-2001-039.